Full paper

Self-doubled-rectification of triboelectric nanogenerator

Sixing Xu [a,b,1], Lei Zhang [a,1], Wenbo Ding [a], Hengyu Guo [a,c], Xiaohong Wang [b,**], Zhong Lin Wang [a,c,d,*]

[a] School of Materials Science and Engineering, Georgia Institute of Technology, Atlanta, GA, 30332-0245, USA
[b] Department of Microelectronics and Nanoelectronics, Tsinghua University, Beijing, 100084, China
[c] Beijing Institute of Nanoenergy and Nanosystems, Chinese Academy of Sciences, China
[d] School of Nanoscience and Technology, University of Chinese Academy of Sciences, Beijing, 100049, China

ABSTRACT

Power management strategies and the corresponding circuits are the unbypassable tough technologies toward practical applications of triboelectric nanogenerators (TENGs). To power electronics, there are two main tasks needed to be tackled for TENG, i.e., to convert the alternating current (AC) to direct current (DC), and to boost the energy output. In this work, we present a power management strategy named Self-doubled-rectification of TENG (SDR-TENG), which is the first AC to DC conversion method delicately customized based on the unique features of TENG. The SDR-TENG divides each operation cycle of the TENG into two periods with different output directions, and keeps the output of one period in the inner capacitor of the TENG and waits until the next period to be released all together. In this way, the voltage output can at most be doubled, the energy output increases two times, and the peak power output can be increased by a factor of four, compared to the traditional bridge rectification, separately. More importantly, SDR-TENG can be easily achieved through only two diodes and work compatibly with all other power management strategies. It is believed that this method may become a standard power management module and can further broaden the applications of TENG devices across fields.

1. Introduction

The prosperity of the distributed portable devices and internet of things (IoTs) has raised the demand of power sources with similar distributed feature [1]. Compared to batteries, harvesting environmental energy in each device to form a self-powered system has significant advantages in the sustainability, environmentally friendly and low-cost operation. Triboelectric nanogenerator (TENG), which can collect environmental and human motion energy, has proven to be an effective power source for self-powered systems and attracted plenty of interests in recent years [2–5]. Enhancing the output performance of TENGs to meet the requirements of electronics is always desirable [6]. The conventional method is to improve the device figure of merit (FOM) by appropriately selecting the pair of triboelectric layers and delicately designing device structure [7–19]. More recently, the power management technologies of TENG, which are more general, has shown its great potential in improving the performance of TENG [20–30].

To make the alternating pulsed output of TENG applicable to electronics, the power management system usually can be divides into three modules [31–33]: the alternating current to alternating current (AC/AC) conversion, the alternating current to direct current (AC/DC) conversion, and the direct current to direct current (DC/DC) conversion (Fig. 1a). Over the past few years, great achievements have been made in the AC/AC and DC/DC conversions of TENG. For example, Xi et al. [26] and Cheng et al. [22] separately proposed synchronized switching systems for the AC/AC conversion of TENG, which make the output approaching the 'cycles for maximum output (CMEO)' limit. Liu et al. and Ghaffarinejad et al. [25] reported the application of Bennet's doubler circuit in the power management of TENG, which can bring an exponential enhancement during the AC/AC conversion. Xu et al. [28] designed a charge supplemental channel using a parallel diode to zero check TENG in each cycle so that the performance can be greatly enhanced. In addition, Park et al. [34] designed a dual-input buck converter circuits for the DC/DC conversion of TENG, which solved the

---

asymmetric output problem of TENG and reduced the energy loss. Despite the works in the AC/AC and DC/DC conversions of TENG, there is no work about the AC/DC module of TENG reported. To our knowledge, all of the existing power management systems of TENG utilizes the full-bridge or half-bridge rectification methods for the AC/DC conversion, which are of no optimization according to the characteristics of TENG.

Herein, in both theory and experimental verification, we first propose an AC/DC conversion method named self-doubled-rectification of TENG (SDR-TENG), which can achieve at most four times of power output compared with bridge rectification, and can solve the asymmetric output problem of TENG for the more common capacitive loads. For the SDR-TENG, each operation cycle is divided into two periods with different output directions. During the operation, the charges of the first period are locked and accumulated in the intrinsic capacitor of TENG, and then together with the charges of the second half cycle be released to the load. In this way, the equivalent voltage of the total transferred charge can be doubled, leading to a two times increase in total energy output and three times improvement in peak power output. Meanwhile, as the positive output and negative output are put together, the energy waste caused by the asymmetric output problem is naturally solved. The SDR-TENG is easily achieved by connecting two diodes to the TENG, even half less than the requirement of a full-wave bridge, and the results fit well with the theory and simulation. More importantly, the optimization of the rectification method in this work is compatible with other works in the AC/AC and DC/DC conversions of TENG. We believe the proposed scheme could broaden the potential applications of TENG in the self-powered systems as an effective power source.

2. Result

2.1. Mechanism and simulation of SDR-TENG

The mechanism of SDR-TENG is illustrated in Fig. 1b and c. As analyzed in previous publications [17], TENG device can be modeled as the series connection of a voltage source and a capacitor. For the conventional full-wave rectification, the output of TENG in the positive and negative cycle directly passes the bridge and applied to the load (Fig. 1b and c). As for the SDR-TENG, in the first period with negative output, the diode D1 is short-circuited and D2 is open-circuited because the lower electrode has higher voltage than the upper electrode. Consequently, the free charges accumulated on the intrinsic capacitor of TENG to balance the intrinsic voltage of TENG. At the second period, the voltage source starts to decrease so that the voltage of the lower electrode is higher than the upper electrode, which results in the open-circuit of D1 and short-circuit of D2. Therefore, during the second period, the output of the voltage source together with the output of the capacitor pass the diode D2 and applied to the load. Originated from the superposition effect of the circuit, the voltage output can be doubled for symmetric input; the power output, which is proportional to the square of the voltage, can be at most increased by four times.

To prove the self-doubling effect, a physical model of TENG is established using COMSOL Analysis, as shown in Fig. 2. For the sake of simplicity and intuition, we choose the free-standing mode TENG. However, it is believed that the self-double effect appeals to all types of TENGs because of the same circuit model. As shown in Fig. 2a, for the operation of bridge rectification, the output voltage of TENG varies with
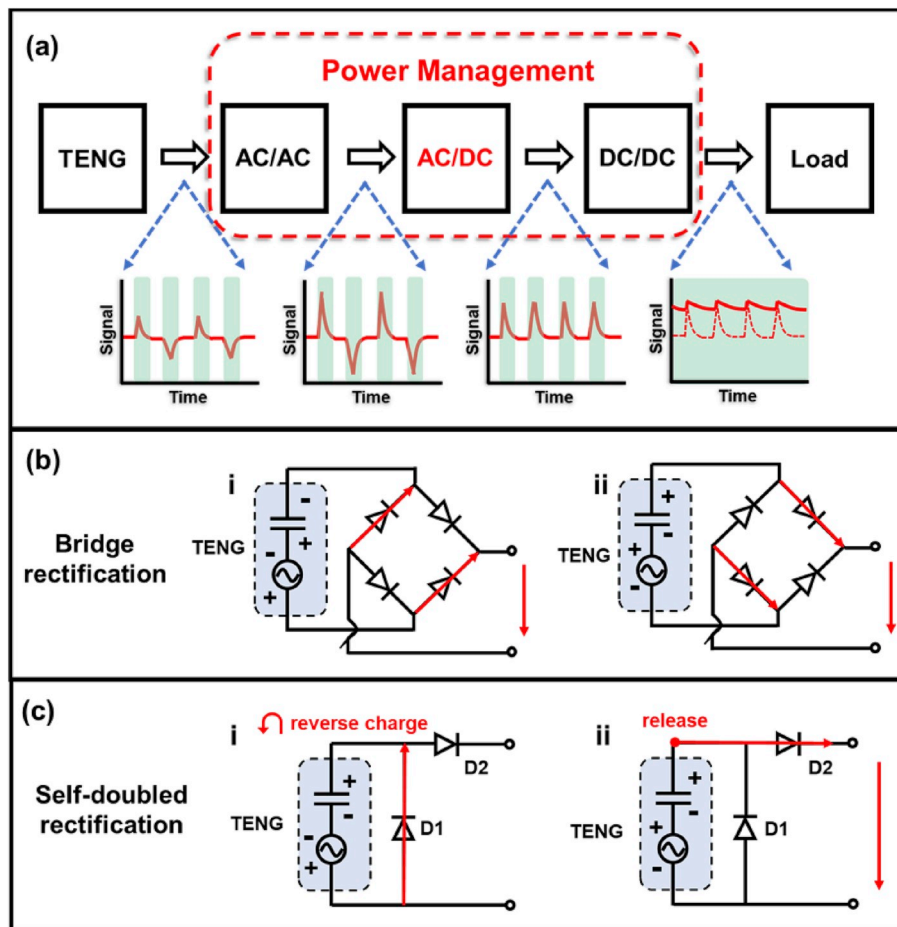

Fig. 1. The concept illustration of the SDR-TENG. (a) The flow of a power management system. (b) The operation of conventional bridge rectification. (c) The operation of SDR-TENG.
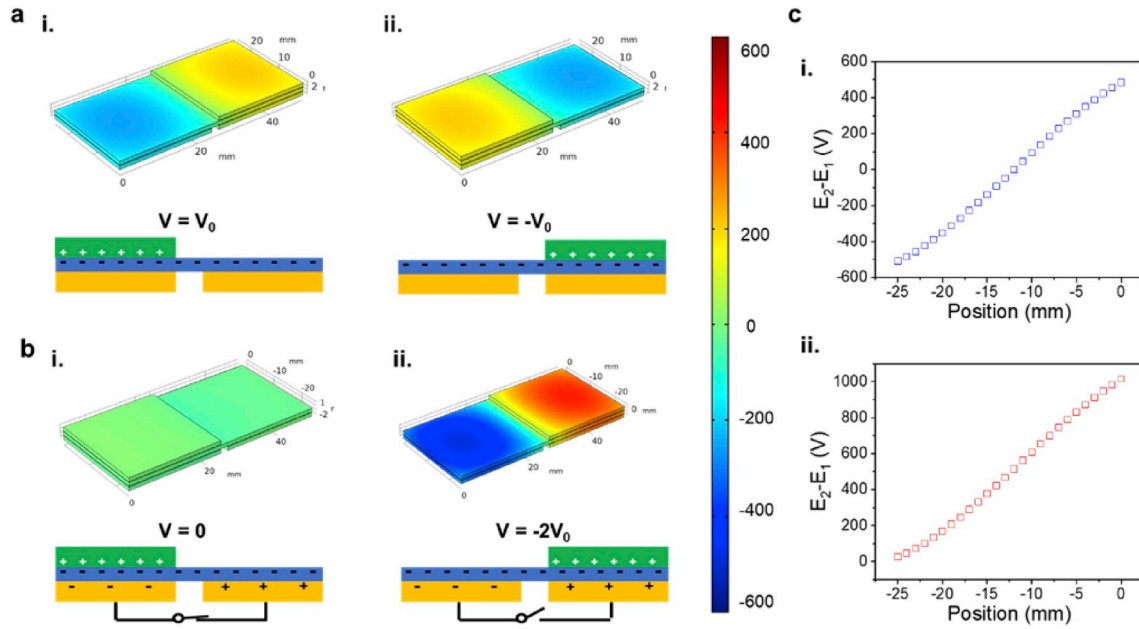
ARTICLE IN PRESS

S. Xu et al.   Nano Energy xxx (xxxx) xxx

Fig. 2. The COMSOL simulation of a free-standing mode TENG for the regular bridge rectification and SDR-TENG. (a) The voltage distribution of the operation of bridge rectification. (b) The voltage distribution of the operation of SDR-TENG. (c) The voltage distribution of (i) bridge rectification and (ii) SDR-TENG.

the motion. For the SDR-TENG, the device is short-circuited in the first period so that the free charges on the conductive layers will be rearranged to balance the voltage, as shown in Fig. 2b(i). After that, the external circuit is open-circuited and the free charges will be isolated on the conductive layers and maintains a voltage difference of V_0. In the second period, the polarized charge moves to another side and forms a doubled voltage. As proven in Fig. 2c, the voltage distribution of SDR-TENG is exactly doubled compared with bridge rectification.

2.2. SDR-TENG for resistive load

To fully demonstrate the advantages of SDR-TENG, the output of SDR-TENG is simulated and compared with the output of regular bridge rectification. A free-standing mode TENG device with parameters listed in Table 1 and a sinusoidal excitation are proposed. Fig. 3a shows the sinusoidal output of TENG without rectification. Apparently, for the full-wave rectification, the positive output of TENG is remained and the negative output of TENG is reversed with a voltage drop of due to the diode, as shown in Fig. 3b. When using SDR-TENG, the output will be cleared when the output of TENG is negative due to the short-circuit brought by the diode. During this period, the intrinsic capacitor is charged to resist the voltage of the polarized charge until the extreme movement point. Afterward, when the output of TENG turns to positive, the diode D1 is open-circuited and the output of TENG will be applied to the load. The voltage applied to the load can be quantitatively calculated by analyzing the state equation of TENG (detailed derivation in *Supplementary Note S1*):

$$V_t = V_o \sin(wt) + V_c e^{\frac{-t}{RC}} \tag{1}$$

where Vo is the open-circuit voltage of the TENG, Vc is the initial voltage of the capacitor at the second period, R is the load resistance and C is the intrinsic capacitance of TENG. It can be observed, different from the

usual sinusoidal voltage, the output of SDR-TENG contains two competing parts: the sinusoidal part contributed by the electric field of polarized charge, and the exponential part contributed by the capacitor discharge. The voltage output of SDR-TENG shown in Fig. 3c is obviously higher than the output of bridge rectification, which only has the sinusoidal part. In addition, there is only one diode-loss. The voltage charge (V-Q) curve is the tool to investigate the output power of TENG. The V-Q curve comparison of bridge rectification and SDR-TENG is shown in Fig. 3d. Although the bridge rectification brings two parts of the energy output, the total transferred charge and maximum voltage are lower than that of SDR-TENG, hence the SDR-TENG brings obviously higher energy output. The improved energy output is originated from the higher input mechanical work to overcome the electrostatics from the doubled electrical field, as proved in Fig. 2.

To investigate the effect of the load resistance, the voltage output of SDR-TENG with various loads are plotted in Fig. 3e. With the increase of the load resistance, the output voltage amplitude gradually grows to twice of the maximum voltage of TENG. Moreover, the duty ratio (the time with output divided by the period) increases from 50% to 100% with the increase of the load resistance. The peak power comparison of bridge rectification and SDR-TENG is plotted in Fig. 3f, which shows that the bridge rectification and SDR-TENG have similar peak power with small load, but SDR-TENG demonstrate as high as four times higher peak power at load resistance larger than matching impedance. This phenomenon is easy to understand through the status Equation (1): with the small load, the charge pre-stored on the intrinsic capacitor will rapidly run away due to the small time constant; while with the large load, the pre-stored charge will be slowly released at high voltage, which brings more power benefit. The energy output can be calculated by the integration of power with time, as detailed in *Supplementary Note S2*. It can be observed that a maximum of three times improvement of energy output can be made by using the SDR-TENG.

A free-standing mode TENG device with the parameters approaching Table 1 is established to verify the proposed theory. The current signal and voltage signal of the resistive loads strictly obey the Ohm's Law. Therefore, to get higher precision, we have measured the current outputs of SDR-TENG and bridge rectification and then obtained the voltage output by multiplying the current with the resistances, as shown in Fig. 4.
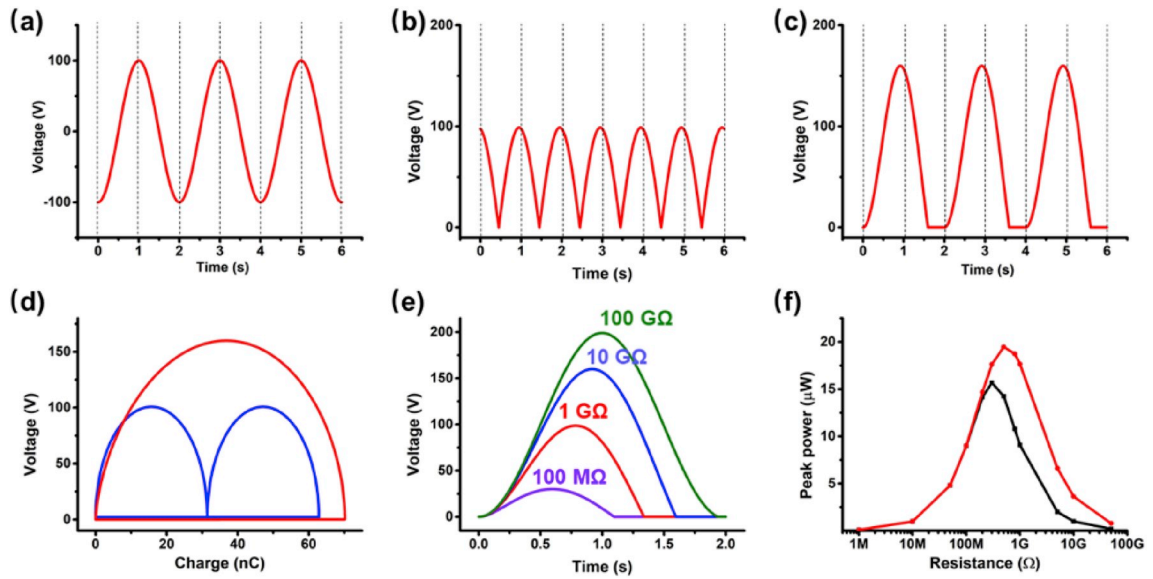
Table 1
Parameters used for simulating the SDR-TENG.

Polarized charge density	Intrinsic capacitance	Area for each electrode	Excitation frequency
50 µC/cm²	0.5 nF	12 cm²	1 Hz

Fig. 3. The simulation of SDR-TENG output under resistive load. (a) The sinusoidal input of SDR-TENG. (b) The output of full-bridge rectification. (c) The output of SDR-TENG for 10G Ω load. (d) The V-Q plot comparison of bridge rectification and SDR-TENG. (e) The voltage output of SDR-TENG under various load resistance. (f) The output power of bridge rectification and SDR-TENG under various load resistance.

When the load resistance is as low as 1G Ω, the output of bridge rectification reaches a voltage amplitude around 55 V (Fig. 4a). Meanwhile, as shown in Fig. 4b, the SDR-TENG brings an output voltage amplitude around 62 V, 12.7% higher than that of bridge rectification.

However, it should be mentioned that the duty ratio of the output of SDR-TENG is only about 60%, which results in the low transferred charge and energy output. The transferred charge of two methods are shown in Fig. 4c, which indicates although SDR-TENG provides higher
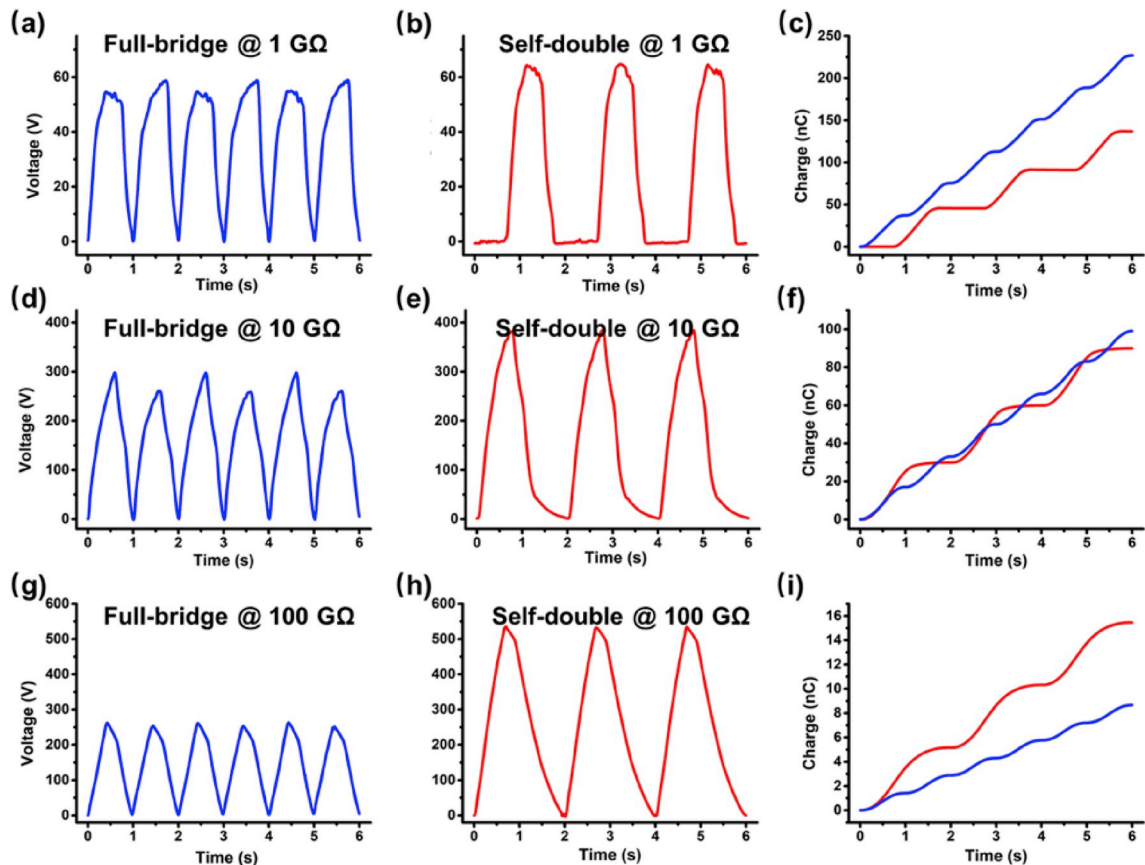

Fig. 4. The experiment results of bridge rectification and SDR-TENG. (a) Voltage output of full-bridge rectification, (b) SDR-TENG and (c) transferred charge comparison under load resistance of 1G Ω. (d) Voltage output of full-bridge rectification, (e) SDR-TENG and (f) transferred charge comparison under load resistance of 10G Ω. (g) Voltage output of full-bridge rectification, (h) SDR-TENG and (i) transferred charge comparison under load resistance of 100G Ω.

S. Xu et al.

voltage (current), the transferred charge is less because of the low duty ratio. When the load grows to 10G Ω, which is the level of the matching impedance, the bridge rectification brings a voltage amplitude around 270 V, as shown in Fig. 4d. The SDR-TENG results in a voltage amplitude to 390 V, which is 44% higher than that of bridge rectification. In addition, the duty ratio increases to 80%. At this situation, the transferred charges of bridge rectification and SDR-TENG are nearly the same. However, the SDR-TENG can provide higher power output due to the higher voltage output. When the load resistance increases to 100G Ω, which is much larger than the matching impedance, the voltage amplitude of SDR-TENG reaches 550 V, which is twice of the bridge rectification, as illustrated in Fig. 4g and h. And the duty ratio is almost 100%, the transferred charge is also more than the bridge rectification. The results fit well with the theory prediction in Fig. 3.

2.3. SDR-TENG for capacitive load

The stable voltage supply is essential for most of electronics. Therefore, in most cases, there should be a filtering capacitor as the first-level load before the electronics as the second-level load, which is illustrated in Fig. 5a. Therefore, we more concern about the performance of SDR-TENG with the capacitive loads.

To evaluate the advantage of SDR-TENG with capacitive loads, the situations should be classified into two categories: the symmetric TENG and asymmetric TENG. For free-standing mode TENG devices, the outputs are almost symmetric. The charging process of bridge rectification can be expressed by Equation (2), while the charging process of SDR-TENG can be expressed by Equation (3) and Equation (4), in which i represents the numbers of half-period (detailed derivation in *Supplementary Note S2*). The charging processes are furtherly plotted in Supplementary Fig. S2, which indicates that the charging of SDR-TENG is slower at first, its stable voltage reaches twice of the bridge rectification. Obviously, the doubled voltage will bring doubled current and four-times increased power for the load electronics.

Fig. 5. The concept illustration for the SDR-TENG under capacitive load. (a) The scheme of a TENG-Rectification-Capacitor system. (b)–(c) The output for (b) full-bridge and (c) SDR-TENG with symmetric output of TENG. (d)–(e) The output for (d) full-bridge and (e) SDR-TENG with asymmetric output of TENG.

$$\frac{V_i}{V_o} = 1 - \left(1 - \frac{1}{n}\right) \times \left(1 - \frac{2}{n}\right)^{i-1} \tag{2}$$

$$\frac{V_i}{V_o} = 2 - 2 \times \left(1 - \frac{1}{n}\right)^{\frac{i-1}{2}} \quad \text{for} \quad i = \text{odd} \tag{3}$$

$$\frac{V_i}{V_o} = 2 - 2 \times \left(1 - \frac{1}{n}\right)^{\frac{i-1}{2}} \quad \text{for} \quad i = \text{even} \tag{4}$$

The asymmetric output of TENG, which occurred widely in the contact-separation mode TENG, single-electrode TENG and sliding mode TENG, is always puzzling for the capacitive load. To maximize the efficiency, we can assume there is an optimized voltage for the load capacitor, and the energy output can be expressed by Equation (5), where Q is the charge provided by the TENG, Q_{total} is the maximum charge the TENG can provide and Q_{wasted} is the charge be retained on the intrinsic capacitor of TENG. Q_{total} and Q_{wasted} can be expressed by Equation (6), where δ is the polarized charge density, S is the area of the electrode and C_{min} is the intrinsic capacitance of TENG when reaches the maximum displacement (i.e. the smallest capacitance). Therefore, the voltage should be stabled at the half of the maximum voltage to get the optimized output. For the asymmetric TENG, if the output of one direction is lower than half of another direction, the lower direction will be fully wasted, just shown in Fig. 4d. However, this problem is naturally solved in the SDR-TENG system because the output of two directions are put together, as shown in Fig. 4e.

$$E = Q \times V_c = (Q_{total} - Q_{wasted}) \times V_c \tag{5}$$

$$Q_{total} = \delta \times S; Q_{wasted} = C_{min} \times V_c$$

$$E = E_{max} = \frac{(\delta \times S)^2}{4 \times C_{min}} \quad when V_c = \frac{\delta \times S}{2 \times C_{min}} \tag{6}$$

To verify the assumption and derivation, a free-standing mode TENG with symmetric output and a contact-separation mode TENG with asymmetric output are fabricated to examine the performance of SDR-TENG. The voltage output of the free-standing mode TENG is plotted in Fig. 6a, showing great symmetry with amplitude around 1200 V. The output of SDR-TENG compared with bridge rectification are investigated. Fig. 6b shows the output of SDR-TENG and bridge rectification with the capacitive load of 100 nF. It is clear to see that although the charging of SDR-TENG is slower than bridge rectification at first, a nearly doubled stable voltage can be achieved, which agrees well with the theory. Fig. 6c demonstrates the comparison with larger capacitor of 500 nF. Similarly, a nearly doubled stable voltage is obtained. The asymmetric voltage output of the contact-separation mode TENG is shown in Fig. 6d, of which the positive amplitude of 900 V and negative amplitude of 400 V. The bridge rectification can bring a stable voltage around 500 V (Fig. 6e) and obviously the negative energy is fully wasted because of the diode bridge. While using SDR-TENG, an average voltage of 700 V is achieved and both directions of the output are used.

It should be mentioned that in the situation of connecting capacitive load, the total energy output of TENG with SDR-TENG is the same as that with the bridge rectification. What becomes higher is the final/stable energy stored in the capacitor. The price is it takes longer time to charge, which can be verified in Fig. 6b (c) and Supplementary Fig. S2.

3. Conclusion

We have developed the first AC/DC conversion strategy for TENG. By continuous switching the diode short-circuit and open-circuit, each operation cycle of TENG is divided into two periods with opposite directions and the energy output is concentrated on one of the periods. In this way, doubled voltage and four-times increased power output can be obtained, and the energy waste caused by the asymmetry problem is
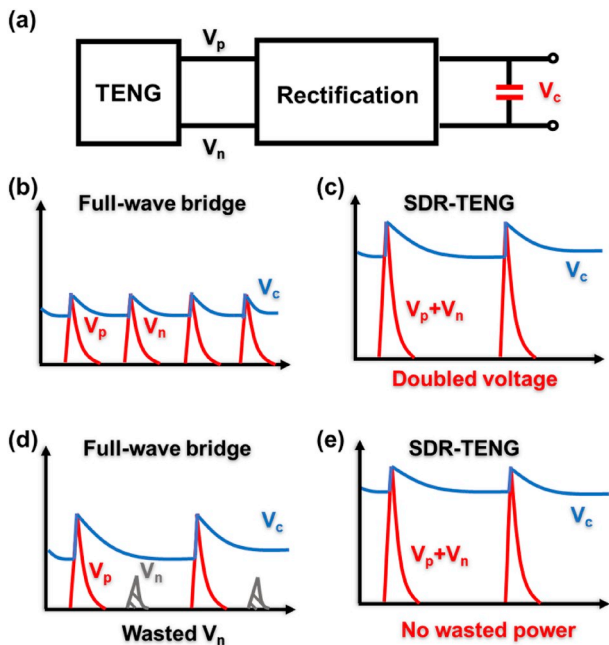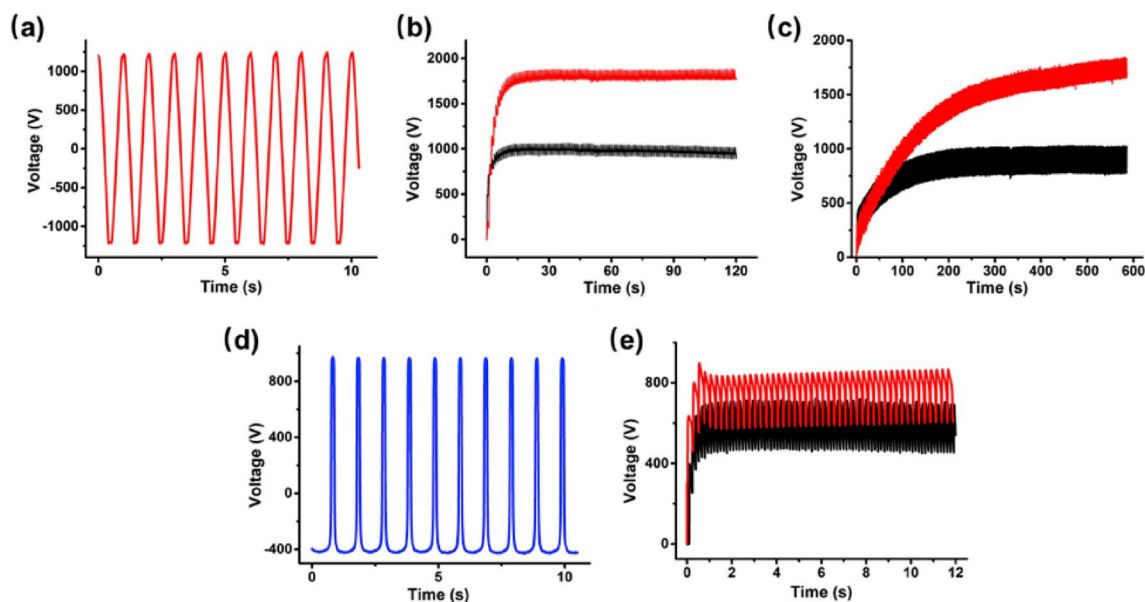
Fig. 6. The experimental outputs for the SDR-TENG and bridge rectification under capacitive load. (a) The output of free-standing TENG. **(b–c)** The output comparison of SDR-TENG (red) and bridge rectification (black) with **(b)** 100 nF and **(c)** 500 nF capacitive loads. **(d)** The output of contact-separation TENG. **(e)** The output comparison of SDR-TENG (red) and bridge rectification (black).

naturally solved. In addition to the theoretical derivation and model simulation, the performance of the SDR-TENG is also experimentally demonstrated. A significant energy improvement is observed compared with SDR-TENG and bridge rectification, especially for large resistive load and small capacitive load. It is believed such a general, low-cost and highly effective power management strategy will soon be applied to various TENG devices and promote the industrialization and commercialization of TENG.

4. Methods

Preparation and operation of the symmetric freestanding TENG device. A typical freestanding device structure was utilized in this project. The static part of this TENG was made of attaching two $3 \times 4 \, cm^2$ aluminum foil rectangular to a $3 \times 9 \, cm^2$ acrylic board first with a separation of 2 mm. Sequentially, the PTFE tape covered all these two Al electrodes onto the acrylic substrate. The movable object was constructed by a 50 μm thickness $3 \times 4 \, cm^2$ nylon film mounted onto another acrylic board, rubber foam as a buffering layer inside to enhance the effective contact area and the output performance. To operate this TENG, the static part and movable object were fixed onto a vertical stage and a linear motor separately and facing each other. With the acceleration of $5 \, m \, s^{-2}$, the motion frequency was kept 1 Hz and no delay time in this process.

Preparation and operation of the asymmetric contact-separation TENG device. This preparation of this device is similar to the freestanding TENG device. In the static part, $3 \times 3 \, cm^2$ PTFE film and Al foil were attached to acrylic board and fixed to a stage. For the movable object, same area Al foil and rubber foam were mounted to another acrylic board. The movable object was actuated by linear motor with the static part with a full contact-separation displacement of 30 mm. In this process, the acceleration is $5 \, m \, s^{-2}$, the motion frequency is 1 Hz, and no delay time.

Electric measurement equipment. The output voltage signals and charge transfer were captured using Keithley 6514 System Electrometers. The functional motion was produced by Linear motor system (Linmot Linear guide H01–37x166/180).

Data availability

The data that support the plots within this paper and other finding of this study are available from the corresponding authors upon reasonable request.

Declaration of competing interest

The authors declare no conflict of interest.

Appendix A. Supplementary data

Supplementary data to this article can be found online at https://doi.org/10.1016/j.nanoen.2019.104165.

References

[1] Z.L. Wang, Entropy theory of distributed energy for internet of things, Nano Energy 58 (2019) 669–672.

[2] Z.L. Wang, J. Chen, L. Lin, Progress in triboelectric nanogenerators as a new energy technology and self-powered sensors, Energy Environ. Sci. 8 (8) (2015) 2250–2282.

[3] C. Wu, A.C. Wang, W. Ding, H. Guo, Z.L. Wang, Triboelectric nanogenerator: a foundation of the energy for the new era, Adv. Energy Mater. 9 (1) (2019) 1802906.

[4] F.R. Fan, Z.Q. Tian, Z.L. Wang, Flexible triboelectric generator, Nano Energy 1 (2) (2012) 328–334.

[5] Z.L. Wang, On Maxwell's displacement current for energy and sensors: the origin of nanogenerators, Mater. Today 20 (2) (2017) 74–82.

[6] W. Ding, A.C. Wang, C. Wu, H. Guo, Z.L. Wang, Human–machine interfacing enabled by triboelectric nanogenerators and tribotronics, Adv. Mater. Technol. 4 (1) (2019) 1800487.

[7] L. Xu, Y.K. Pang, C. Zhang, T. Jiang, X.Y. Chen, J.J. Luo, W. Tang, X. Cao, Z. L. Wang, Integrated triboelectric nanogenerator array based on air-driven membrane structures for water wave energy harvesting, Nano Energy 31 (2017) 351–358.

[8] C. Xu, A.C. Wang, H. Zou, B. Zhang, C. Zhang, Y. Zi, L. Pan, P. Wang, P. Feng, Z. Lin, Raising the working temperature of a triboelectric nanogenerator by quenching down electron thermionic emission in contact-electrification, Adv. Mater. 30 (38) (2018) 1803968.

[9] C. Xu, Y. Zi, A.C. Wang, H. Zou, Y. Dai, X. He, P. Wang, Y.C. Wang, P. Feng, D. Li, On the electron-transfer mechanism in the contact-electrification effect, Adv. Mater. 30 (15) (2018) 1706790.

[10] J. Peng, S.D. Kang, G.J.J. Snyder, Optimization principles and the figure of merit for triboelectric generators, Sci. Adv. 3 (12) (2017), eaap8576.

[11] J. Shao, T. Jiang, W. Tang, X. Chen, L. Xu, Z.L. Wang, Structural figure-of-merits of triboelectric nanogenerators at powering loads, Nano Energy 51 (2018) 688–697.

[12] Y. Zi, S. Niu, J. Wang, Z. Wen, W. Tang, Z.L. Wang, Standards and figure-of-merits for quantifying the performance of triboelectric nanogenerators, Nat. Commun. 6 (2015) 8376.

[13] J. Wang, S. Li, F. Yi, Y. Zi, J. Lin, X. Wang, Y. Xu, Z.L. Wang, Sustainably powering wearable electronics solely by biomechanical energy, Nat. Commun. 7 (2016) 12744.

[14] J. Wang, C. Wu, Y. Dai, Z. Zhao, A. Wang, T. Zhang, Z.L. Wang, Achieving ultrahigh triboelectric charge density for efficient energy harvesting, Nat. Commun. 8 (1) (2017) 88.

[15] F. Yi, X. Wang, S. Niu, S. Li, Y. Yin, K. Dai, G. Zhang, L. Lin, Z. Wen, H. Guo, A highly shape-adaptive, stretchable design based on conductive liquid for energy harvesting and self-powered biomechanical monitoring, Sci. Adv. 2 (6) (2016), e1501624.

[16] K. Dong, J. Deng, Y. Zi, Y.C. Wang, C. Xu, H. Zou, W. Ding, Y. Dai, B. Gu, B. Sun, 3D orthogonal woven triboelectric nanogenerator for effective biomechanical energy harvesting and as self-powered active motion sensors, Adv. Mater. 29 (38) (2017) 1702648.

[17] S. Niu, Y.S. Zhou, S. Wang, Y. Liu, L. Lin, Y. Bando, Z.L. Wang, Simulation method for optimizing the performance of an integrated triboelectric nanogenerator energy harvesting system, Nano Energy 8 (2014) 150–156.

[18] S. Niu, Y. Liu, X. Chen, S. Wang, Y.S. Zhou, L. Lin, Y. Xie, Z.L. Wang, Theory of freestanding triboelectric-layer-based nanogenerators, Nano Energy 12 (2015) 760–774.

[19] C. Wu, R. Liu, J. Wang, Y. Zi, L. Lin, Z.L. Wang, A spring-based resonance coupling for hugely enhancing the performance of triboelectric nanogenerators for harvesting low-frequency vibration energy, Nano Energy 32 (2017) 287–293.

[20] S. Niu, Y. Liu, Y.S. Zhou, S. Wang, L. Lin, Z.L. Wang, Optimization of triboelectric nanogenerator charging systems for efficient energy harvesting and storage, IEEE Trans. Electron Devices 62 (2) (2015) 641–647.

[21] S. Niu, X. Wang, F. Yi, Y.S. Zhou, Z.L. Wang, A universal self-charging system driven by random biomechanical energy for sustainable operation of mobile electronics, Nat. Commun. 6 (2015) 8975.

[22] X. Cheng, L. Miao, Y. Song, Z. Su, H. Chen, X. Chen, J. Zhang, H. Zhang, High efficiency power management and charge boosting strategy for a triboelectric nanogenerator, Nano Energy 38 (2017) 438–446.

[23] Y. Zi, H. Guo, J. Wang, Z. Wen, S. Li, C. Hu, Z.L. Wang, An inductor-free auto-power-management design built-in triboelectric nanogenerators, Nano Energy 31 (2017) 302–310.

[24] Y. Zi, J. Wang, S. Wang, S. Li, Z. Wen, H. Guo, Z.L. Wang, Effective energy storage from a triboelectric nanogenerator, Nat. Commun. 7 (2016) 10987.

[25] A. Ghaffarinejad, J.Y. Hasani, R. Hinchet, Y. Lu, H. Zhang, A. Karami, D. Galayko, S.-W. Kim, P. Basset, A conditioning circuit with exponential enhancement of output energy for triboelectric nanogenerator, Nano Energy 51 (2018) 173–184.

[26] F. Xi, Y. Pang, W. Li, T. Jiang, L. Zhang, T. Guo, G. Liu, C. Zhang, Z.L. Wang, Universal power management strategy for triboelectric nanogenerator, Nano Energy 37 (2017) 168–176.

[27] H. Qin, G. Cheng, Y. Zi, G. Gu, B. Zhang, W. Shang, F. Yang, J. Yang, Z. Du, Z. L. Wang, High energy storage efficiency triboelectric nanogenerators with unidirectional switches and passive power management circuits, Adv. Funct. Mater. (2018) 1805216.

[28] L. Xu, H. Wu, G. Yao, Li Chen, X. Yang, B. Chen, X. Huang, W. Zhong, X. Chen, Z. Yin, Z.L. Wang, Giant voltage enhancement via triboelectric charge supplement channel for self-powered electroadhesion, ACS Nano 12 (2018) 10262–10271.

[29] J. Cheng, Wen Ding, Y. Zi, Y. Lu, L. Ji, F. Liu, C. Wu, Z.L. Wang, Triboelectric microplasma powered by mechanical stimuli, Nat. Commun. 9 (2018) 3733.

[30] S. Xu, W. Ding, H. Guo, X. Wang, Z.L. Wang, Boost the performance of triboelectric nanogenerators through circuit oscillation, Adv. Energy Mater. 9 (2019) 1900772.

[31] S. Du, A.A. Seshia, in: A Fully Integrated Split-Electrode Synchronized-Switch-Harvesting-On-Capacitors (SE-SSHC) Rectifier for Piezoelectric Energy Harvesting with between 358% and 821% Power-Extraction Enhancement, Solid-State Circuits Conference, 2018.

[32] Y.K. Ramadass, Chandrakasan, An efficient piezoelectric energy harvesting interface circuit using a bias-flip rectifier and shared inductor, IEEE J. Solid State Circuits 45 (1) (2009) 189–204.

[33] Y.C. Shu, I.C. Lien, W. Wu, An improved analysis of the SSHI interface in piezoelectric energy harvesting, Smart Mater. Struct. 16 (6) (2007) 2253.

[34] I. Park, J. Maeng, D. Lim, M. Shim, J. Jeong, C. Kim, in: A 4.5-to-16μW Integrated Triboelectric Energy-Harvesting System Based on High-Voltage Dual-Input Buck Converter with MPPT and 70V Maximum Input Voltage, Solid-State Circuits Conference, 2018.